Short Article

Cell Stem Cell

Patient Adipose Stem Cell-Derived Adipocytes Reveal Genetic Variation that Predicts Antidiabetic Drug Response

Graphical Abstract

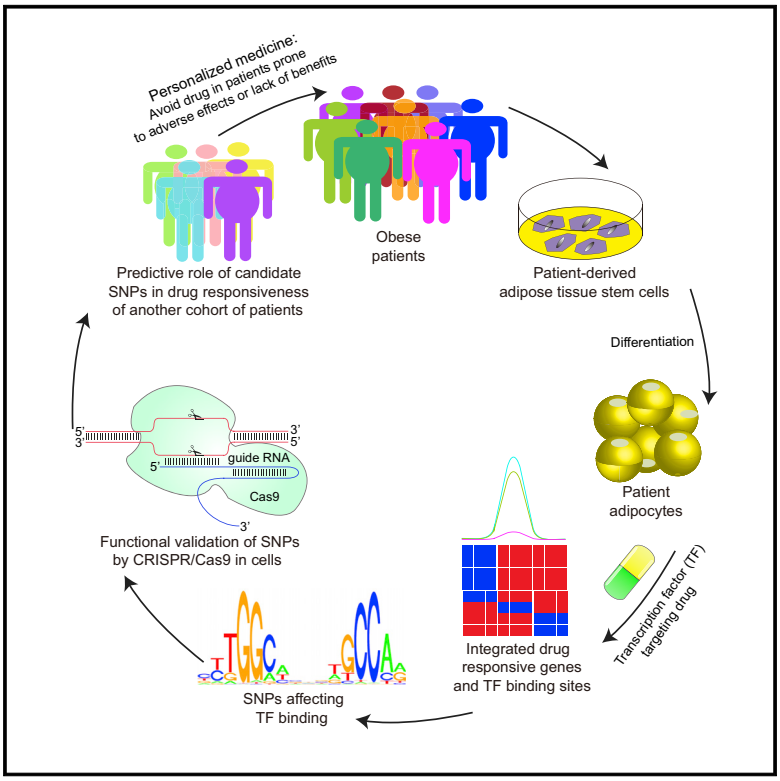

Highlights

- Patient stem cell-derived adipocytes differentially respond to antidiabetic drugs
- Drug responses are governed by genomic binding of PPARγ
- Patient-specific PPARγ genomic binding is controlled by genetic variation
- Genetic variation determines and predicts individual drug responsiveness

Authors

Wenxiang Hu, Chunjie Jiang, Dongyin Guan, ..., Weiping Jia, Raymond E. Soccio, Mitchell A. Lazar

Correspondence

lazar@pennmedicine.upenn.edu

In Brief

Hu, Jiang, et al. utilize patient adipose stem cell-derived adipocytes to reveal SNPs that modulate the effects of antidiabetic drugs by controlling genomic binding of PPARγ.

Hu et al., 2019, Cell Stem Cell *24*, 299–308
February 7, 2019
https://doi.org/10.1016/j.stem.2018.11.018

CellPress

Cell Stem Cell
Short Article

Patient Adipose Stem Cell-Derived Adipocytes Reveal Genetic Variation that Predicts Antidiabetic Drug Response

Wenxiang Hu,[1,2,7] Chunjie Jiang,[1,2,7] Dongyin Guan,[1,2] Pieterjan Dierickx,[1,2] Rong Zhang,[3] Arden Moscati,[5] Girish N. Nadkarni,[5] David J. Steger,[1,2] Ruth J.F. Loos,[5,6] Cheng Hu,[3,4] Weiping Jia,[3] Raymond E. Soccio,[1,2] and Mitchell A. Lazar[1,2,8,*]

[1]Institute for Diabetes, Obesity, and Metabolism, Perelman School of Medicine at the University of Pennsylvania, Philadelphia, PA 19104, USA
[2]Division of Endocrinology, Diabetes, and Metabolism, Department of Medicine, University of Pennsylvania Perelman School of Medicine, Philadelphia, PA 19104, USA
[3]Shanghai Diabetes Institute, Shanghai Key Laboratory of Diabetes Mellitus, Shanghai Clinical Center for Diabetes, Shanghai Jiao Tong University Affiliated Sixth People's Hospital, Shanghai 200233, China
[4]Institute for Metabolic Disease, Fengxian Central Hospital Affiliated to Southern Medical University, Shanghai 201499, China
[5]The Charles Bronfman Institute for Personalized Medicine, Icahn School of Medicine at Mount Sinai, New York, NY 10029, USA
[6]The Mindich Child Health and Development Institute, Icahn School of Medicine at Mount Sinai, New York, NY 10029, USA
[7]These authors contributed equally
[8]Lead Contact
*Correspondence: lazar@pennmedicine.upenn.edu
https://doi.org/10.1016/j.stem.2018.11.018

SUMMARY

Thiazolidinedione drugs (TZDs) target the transcriptional activity of peroxisome proliferator activated receptor γ (PPARγ) to reverse insulin resistance in type 2 diabetes, but side effects limit their clinical use. Here, using human adipose stem cell-derived adipocytes, we demonstrate that SNPs were enriched at sites of patient-specific PPARγ binding, which correlated with the individual-specific effects of the TZD rosiglitazone (rosi) on gene expression. Rosi induction of *ABCA1*, which regulates cholesterol metabolism, was dependent upon SNP rs4743771, which modulated PPARγ binding by influencing the genomic occupancy of its cooperating factor, NFIA. Conversion of rs4743771 from the inactive SNP allele to the active one by clustered regularly interspaced short palindromic repeats (CRISPR)/Cas9-mediated editing rescued PPARγ binding and rosi induction of *ABCA1* expression. Moreover, rs4743771 is a major determinant of undesired serum cholesterol increases in rosi-treated diabetics. These data highlight human genetic variation that impacts PPARγ genomic occupancy and patient responses to antidiabetic drugs, with implications for developing personalized therapies for metabolic disorders.

INTRODUCTION

Obesity has reached global epidemic proportions and is a major risk factor for type 2 diabetes (Caballero, 2007). The nuclear receptor peroxisome proliferator activated receptor γ (PPARγ) is required for adipogenesis and is the target of antidiabetic thiazolidinedione (TZD) drugs (Chawla and Lazar, 1994). TZDs are the only drugs that can reverse the insulin resistance central to the pathophysiology of type 2 diabetes and prevent the development of diabetes and ameliorate cardiovascular complications (Soccio et al., 2014). However, a barrier to progress is that TZDs have notable side effects that limit their routine use, including weight gain, edema, and bone loss (Soccio et al., 2014). Moreover, individuals respond to TZDs differently, such that 20%–30% of diabetic patients fail to respond to TZDs (Sears et al., 2009). Thus, understanding the underlying mechanisms driving a differential response to TZDs could inform personalized and precision approaches to the treatment of type 2 diabetes and associated metabolic diseases.

Here, we used human adipose stem cell (hASC)-derived adipocytes to demonstrate that genetic variation modulates human TZD responses by affecting the genomic occupancy of PPARγ.

RESULTS

hASC-Derived Adipocytes Differentially Respond to Rosiglitazone Treatment

We initially isolated ASCs from subcutaneous adipose tissue of five obese patients (Figures 1A and S1A). hASCs were differentiated to adipocytes in well-defined adipogenic differentiation medium for 2 weeks and then cultured in maintenance medium for 1 week (Figure 1B). After 21 days, we evaluated their adipogenic differentiation efficiency based on morphology, lipid content, and gene expression. Neutral lipid content, measured by oil red O staining, was comparable in all five hASC-derived adipocytes (Figure S1B). The adipocyte marker genes fatty acid binding protein 4 (FABP4) and PPARγ were also expressed at similar levels (Figures S1B and S1C). These five hASC-derived adipocytes with similar properties were used as models to test antidiabetic drug response.

We next treated the hASC-derived adipocytes with the potent TZD rosiglitazone (rosi) for 48 hr beginning at day 21 (Figure 1B).

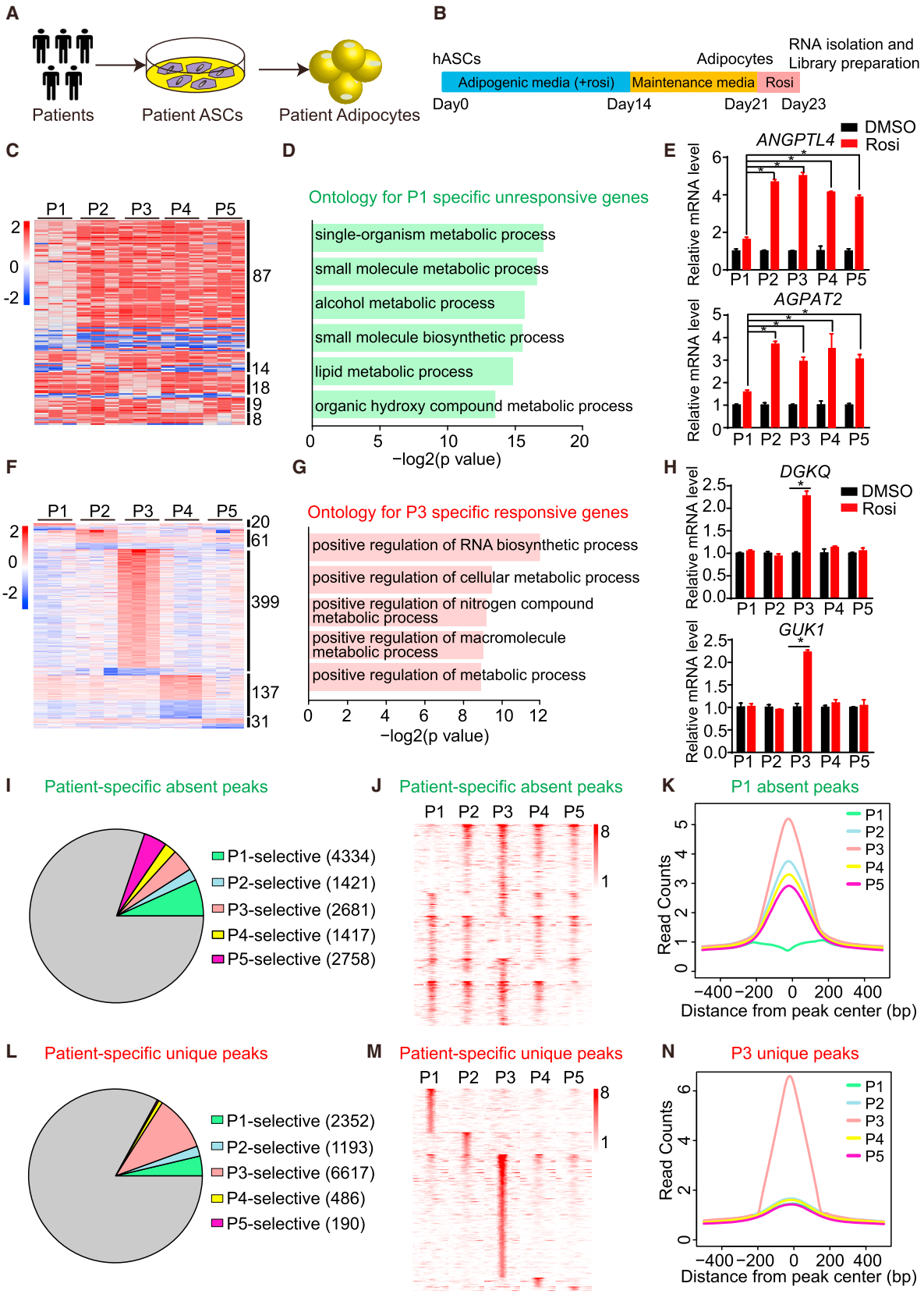

(legend on next page)

Biological replicates of adipocytes differentiated from different aliquots of hASCs from each patient on different days had reproducible transcriptomes (Figure S2A), with 304 genes commonly regulated by rosi (Figures S2B and S2E). Gene ontology (GO) and Kyoto Encyclopedia of Genes and Genomes (KEGG) analysis showed that, as expected, the upregulated genes were enriched for lipid metabolic process and PPAR signaling pathway (Figures S2C and S2H). Among the notable genes commonly induced by rosi, we verified the classic PPARγ-responsive genes *FABP4* and *ADIPOQ* using qRT-PCR (Figure S2D).

Remarkably, besides the commonly regulated genes, we also found 136 genes that were unresponsive to rosi treatment in adipocytes derived from only one of the five patients (Figures 1C and S2F). Patient P1 had the greatest number of patient-specific unresponsive genes, and these 87 genes were enriched for multiple metabolic processes and pathways (Figures 1D and S2I). Of note, genes regulating glucose homeostasis and lipid metabolism, angiopoietin-like 4 (*ANGPTL4*) and 1-acylglycerol-3-phosphate *O*-acyltransferase 2 (*AGPAT2*), were less responsive in patient P1 (Figure 1E). Conversely, we found that 648 genes were uniquely regulated by rosi, 399 of which specifically responded to rosi in patient P3 (Figures 1F and S2G). GO and KEGG analysis showed that P3-specific responsive genes were enriched in metabolic processes and pathways (Figures 1G and S2J). We further confirmed using qRT-PCR that two metabolic genes, diacylglycerol kinase theta (*DGKQ*) and guanylate kinase 1 (*GUK1*), were specifically induced by rosi in patient P3 adipocytes (Figure 1H). Collectively, these data demonstrate that patient-derived adipocytes differentially respond to rosi treatment, recapturing individual differences in the effects of rosi among patients.

Patient-Specific PPARγ Cistromes in hASC-Derived Adipocytes

Since rosi is a potent activating ligand of PPARγ, we next examined whether PPARγ genomic binding is different in these patient hASC-derived adipocytes. PPARγ chromatin immunoprecipitation sequencing (ChIP-seq) in the hASC-derived adipocytes from five patients revealed 12,600 PPARγ-binding sites shared among patients (Figure S3A), with comparable binding intensity (Figures S3B and S3C). The genes near these common sites were enriched for PPAR signaling pathway and fatty acid metabolism (Figure S3D). Strikingly, genomic binding of PPARγ was also patient specific. In each patient's adipocytes, we found that some PPARγ-binding sites were specifically absent (Figures 1I–1K). Notably, patient P1 had the greatest number of sites at which PPARγ binding was uniquely absent (Figure 1I), consistent with the unresponsive gene activation in patient P1 adipocytes based on the earlier transcriptome analysis (Figure 1C).

In contrast, we also identified unique PPARγ-binding sites in each patient's adipocytes. Specifically, patient P3 had the most unique PPARγ-binding sites (Figures 1L–1N), which is also consistent with our previous finding that patient P3 adipocytes activate more genes in response to rosi treatment (Figure 1F). KEGG pathway analysis showed that the genes near these patient P1- and P3-specific sites were enriched for insulin resistance and the adipocytokine signaling pathway, respectively (Figures S3E and S3F). We also found many sites unique to two or three patients (Figures S3G–S3I). Overall, these studies revealed that a fraction of genomic PPARγ binding is different among patient adipocytes, which correlate with their responsiveness to rosi treatment.

To test whether patient-specific hASC-derived adipocytes faithfully reflect adipose tissue biology, we performed transcriptome profiling and PPARγ ChIP-seq on subcutaneous adipose tissue from the same patients. Patient-specific genes and PPARγ cistromes were closely correlated between isogenic adipose tissues and corresponding adipocytes (Figures S3J and S3K), confirming the utility of studying hASC-derived adipocytes as a platform for patient-specific transcription factor binding and drug responses.

Differential PPARγ Binding Drives Patient-Specific Rosi Responses

To determine whether the differential genomic PPARγ binding affects individual rosi responses, we associated patient-specific peaks with patient-specific genes. Interestingly, patient-specific rosi-unresponsive genes, especially patient P1-specific rosi-unresponsive genes, were much more likely to be near PPARγ-absent binding sites (Figure 2A). As an example, the *SLC7A10* gene, which has a metabolic function in adipocytes (Ussar et al., 2014), did not respond to rosi in patient P1 adipocytes (Figure 2B), consistent with a weaker upstream PPARγ-binding site (Figure 2C). Conversely, patient-specific rosi-responsive genes

Figure 1. Differential Rosi Responsiveness and PPARγ Genomic Occupancy in Patient-Specific hASC-Derived Adipocytes

(A) Experimental design of derivation of patient adipocytes.

(B) Scheme of adipogenic differentiation procedure and rosi treatment.

(C) Heatmap of patient-specific unresponsive genes that are not regulated by rosi in only one patient.

(D) Gene ontology for patient P1-specific unresponsive genes.

(E) mRNA expression of patient P1-specific unresponsive genes *ANGPTL4* and *AGPAT2* in adipocytes from five patients, normalized to *HPRT*; DMSO was set to 1, as measured by qRT-PCR.

(F) Heatmap of patient-specific responsive genes that are significantly regulated by rosi in only one patient.

(G) Gene ontology for patient P3-specific responsive genes.

(H) mRNA expression of the patient P3-specific responsive genes *DGKQ* and *GUK1* in adipocytes from five patients, normalized to *HPRT*; DMSO was set to 1, as measured by qRT-PCR.

(I and J) Proportion (I) and heatmap (J) of patient-specific absent peaks that are specifically absent in only one patient, with at least 2-fold fewer reads in one patient compared to the four other patients.

(K) For P1-specific absent peaks, the average binding profiles are shown in 1 kb windows across patients.

(L and M) Proportion (L) and heatmap (M) of patient-specific unique peaks that are specifically unique in only one patient, with at least 2-fold more reads in one patient compared to other four patients.

(N) For P3-specific unique peaks, the average binding profiles are shown in 1 kb windows across patients.

RT-qPCR data are expressed as mean ± SEM. *$p < 0.05$ (Student's t test). n = 3 per group. See also Figures S1–S3.

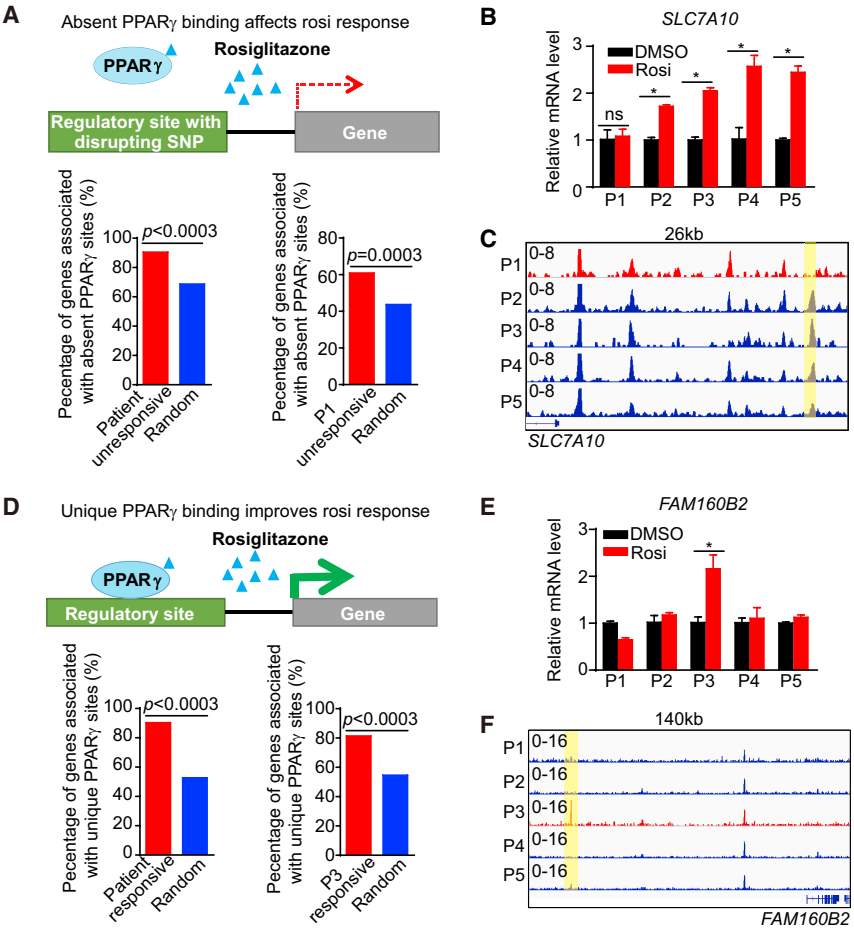

Figure 2. Differential PPARγ Binding Drives Patient-Specific Rosi Responses

(A) Diagram depicting the association between patient-specific absent PPARγ peaks and patient-specific unresponsive genes (top). Percentage of patient-specific unresponsive genes surrounded by patient-specific absent peaks within 200 kb (bottom). p values are determined by random test.

(B) mRNA expression of *SLC7A10* in adipocytes from five patients, normalized to *HPRT*; DMSO was set to 1, as measured by qRT-PCR.

(C) Visualization of a P1-specific absent PPARγ peak region (yellow box) at *SLC7A10* loci across patients using the Integrative Genomics Viewer (IGV).

(D) Diagram depicting the association between patient-specific unique PPARγ peaks and patient-specific responsive genes (top). Percentage of patient-specific responsive genes surrounded by patient-specific unique peaks within 200 kb (bottom). p values are determined by random test.

(E) mRNA expression of *FAM160B2* in adipocytes from five patients, normalized to *HPRT*, DMSO was set to 1, as measured by RT-qPCR.

(F) Visualization of a P3-specific PPARγ peak region (yellow box) at *FAM160B2* loci across patients.

qRT-PCR data are expressed as mean ± SEM. * $p < 0.05$; ns, $p > 0.05$ (Student's t test). n = 3 per group.

tended to have patient-specific PPARγ-binding sites nearby (Figure 2D). For example, the gene *FAM160B2* was specifically induced by rosi in patient P3 (Figure 2E). Consistent with this, we also found that upstream PPARγ binding was also stronger in P3 than in other patient adipocytes (Figure 2F). Genome-wide, integration of SNPs from dbSNP150 with patient-specific PPARγ-binding sites revealed that SNPs occurred more frequently than would be expected by chance in individual patient-specific sites of absent binding and unique binding, but not at common PPARγ-binding sites, where SNPs were, if anything, less frequent than by chance (Figure S4A). These data indicate that patient-specific responses to rosi are determined by individual differences in PPARγ genomic binding.

Rosi Response of the Cholesterol Metabolism Gene *ABCA1* Is Determined by SNP rs4743771

We identified a total of 129 SNPs located in PPARγ-binding sites that were absent in P1 or unique to P3 and also predicted to have a strong effect on the binding motif for PPARγ or transcription factors previously shown to cooperatively support PPARγ binding (C/EBPα, NFI, or GR) (Soccio et al., 2015). SNP rs4743771 was of particular interest, because it had a major effect on PPARγ binding and was in the vicinity of the PPARγ-regulated *ABCA1* gene (Chawla et al., 2001), whose protein product regulates reverse cholesterol transport (Oram and Lawn, 2001). We therefore focused on this SNP as proof of concept for functional testing of genetic variants in individual response to drug therapies.

Patient P1 was uniquely homozygous for the minor A allele (A/A) (minor allele frequency [MAF], A = 0.4012, 1000 Genomes), while all of the other four patients had at least one C allele, with 3 being C/C (Figure 3A). Patient P1 had a weaker PPARγ peak in the genomic region spanning rs4743771, and this result was further confirmed by PPARγ ChIP-qPCR (Figure 3B). Rosi had very little effect on PPARγ binding in all patients, as has been previously found in mouse adipocytes (Step et al., 2014). Remarkably, however, rosi induced *ABCA1* gene expression in every patient except patient P1, who carried the A/A genotype (Figure 3C). Chromosome conformation capture (3C) in patient-derived adipocytes demonstrated the existence of a chromatin loop connecting the region near rs4743771 and the *ABCA1* gene promoter (Figure 3D). The chromatin looping was stronger in C/C patient adipocytes (Figure 3E), and while this did not alter basal gene expression, it may contribute to the ability of rosi to induce transcription from this PPARγ-bound enhancer.

The transcriptional importance of rs4743771 was assessed using luciferase reporter assays in mouse 3T3-L1 adipocytes. Consistent with the activity of the C allele in the native gene, this sequence conferred rosi responsiveness to a reporter gene carrying the C allele, whereas the A did not (Figure 3F). Since the PPARγ-binding-dependent genotype/rosi-response phenotype relationship was not unique to the *ABCA1* locus, we tested additional examples, including the A allele at SNP rs2106146 (MAF, G = 0.4083, 1000 Genomes) which conferred

rosi responsiveness to the *SLC25A1* gene (Figure 3G) and the A allele at SNP rs76932545 (MAF, A = 0.0266, 1000 Genomes) which was critical for rosi responsiveness of the *MSX1* gene (Figure 3H). In both cases, the allele correlating with rosi-induced gene expression was found to be uniquely active in the ability of rosi to drive expression of a reporter gene (Figure 3I). These results clearly demonstrate predictable modulation of PPARγ occupancy and rosi response by genetic variation.

Variation in rs4743771 Controls PPARγ Function by Modulating NFIA Binding

To understand how rs4743771 regulates PPARγ genomic binding, we examined its potential effects on the PPARγ motif as well as the motifs for nearby PPARγ cooperating transcription factors. Although rs4743771 does not affect a PPARγ motif, it has a major effect on a motif predicted to be a binding site for NFI, a transcription factor that has been shown to cooperate with PPARγ at the genome (Hiraike et al., 2017; Soccio et al., 2015). Intriguingly, the score of agreement with the NFI consensus motif was ~17 greater for the C allele than for the A allele (Figure 3J). To test this, we performed NFI ChIP-qPCR in adipocytes from 3 A/A patients and 3 C/C patients. Indeed, adipocytes with the C/C genotype displayed much greater NFI binding at this site in the *ABCA1* locus than adipocytes from A/A patients (Figure 3K). In contrast, NFI binding was genotype independent on an unrelated NFI-binding region (*ALAS2*). Moreover, knockdown of NFIA impaired the rosi-induced *ABCA1* gene expression (Figure 3L). The effect of NFIA was genome-wide, such that NFIA deletion abrogated the induction of 104 genes in rosi-treated adipocytes (Figure 3M). Consistent with this, ~8% of patient-specific PPARγ-binding sites contained SNPs that altered NFI-binding motifs, which was similar to the percentage of patient-specific PPARγ binding at sites where the SNP affected the PPARγ-binding motif itself (Figure S3L).

Genome Editing Confers PPARγ Binding and Rosi Response at *the ABCA1* Locus

To determine whether the C allele is sufficient to convey rosi responsiveness to the *ABCA1* gene, we next used clustered regularly interspaced short palindromic repeats (CRISPR)/Cas9 to edit rs4743771. For this purpose, we used the SGBS human preadipocyte cell line (Fischer-Posovszky et al., 2008), which is more highly proliferative and thus more amenable to gene editing than patient-derived ASCs. We found SGBS to be homozygous for the rosi-unresponsive A/A genotype, and PPARγ binding was weak in the genomic region spanning rs4743771, similar to what was observed in adipocytes from patient P1 (Figure 3A). Importantly, we also noted that *ABCA1* gene expression was not induced by rosi in SGBS-differentiated adipocytes (Figure S4B). The replacement of A allele of SGBS cells into the C allele (A > C) was confirmed by Sanger sequencing (Figure 4A). The A > C-edited SGBS cells retained the ability of SGBS to differentiate into adipocytes (Figure S4C). Remarkably, SGBS cells that underwent A > C editing acquired PPARγ binding at the *ABCA1* locus with no change at positive and negative control sites (Figure 4B). Moreover, they also acquired NFI binding selectively at this locus (Figure 4C), again with no change at an unrelated binding site near the *ALAS2* gene as well as a negative control site, consistent with the conclusion that this genetic variant directly alters binding of this PPARγ cooperating factor, which in turn affects responsiveness to rosi.

Functionally, rosi induced higher *ABCA1* expression in A > C-edited SGBS cells (Figure 4D). By contrast, basal expression of *ABCA1* was unchanged, and liver X receptor (LXR) agonist T091317, a known inducer of *ABCA1* by a different mechanism (Chawla et al., 2001), induced *ABCA1* similarly in both wild-type and edited adipocytes (Figure 4D). Moreover, genome editing did not affect the ability of rosi to induce *FABP4*, another PPARγ target gene (Figure S4D). Thus, the C allele of rs4743771 is sufficient to support NFIA and PPARγ binding and convey rosi responsiveness to the *ABCA1* gene.

Rosi Transcriptional Responses Can Be Predicted from Genome Information

Based on the above results, we prospectively tested 20 additional patients (4 A/A, 11 A/C, and 5 C/C patients) to see whether the genotype of SNP rs4743771 is predictive of rosi responsiveness of *ABCA1*. As predicted from the analysis of the initial 5 patients, C/C patient adipocytes consistently responded to rosi with ~2-fold induction of *ABCA1*, while A/A patients did not (Figure 4E). Moreover, A/C heterozygotes had intermediate responses to rosi, suggesting gene-dosage effects of this allele. By contrast rs4743771 genotypes were unrelated to basal *ABCA1* gene expression (Figure S4E), indicating that factors other than PPARγ likely drive basal *ABCA1* transcription.

Genetic Variation at rs4743771 Controls the Effect of Rosi on Cholesterol Metabolism in Patient Adipocytes

Since ABCA1 is regulator of cholesterol efflux, we next explored whether SNP rs4743771 also affects cholesterol metabolism. Notably, we found that rosi induced cholesterol efflux from adipocytes to serum in C/C patient adipocytes but was ineffective in A/A patient adipocytes (Figure 4F). As a control, T091317 similarly induced cholesterol efflux in patient adipocytes of either genotype. Thus, the SNP that is permissive for rosi induction of *ABCA1* by altering PPARγ binding predictably controlled whether a PPARγ ligand altered lipid metabolism, whereas the effects of an LXR ligand were independent of the specific rs4743771 allele.

Similarly, as *SLC25A1* encodes a citrate transporter that is important for mitochondrial metabolism (Hlouschek et al., 2018), we also examined whether the effect of rosi on the mitochondrial function of patient-derived adipocytes was differentially affected by the rs2106146 genotype. Indeed, the G/G-patient-derived adipocytes with reduced PPARγ binding and rosi induction of *SLC25A1* exhibited an impaired effect of rosi on both basal (Figure S4F) and maximal mitochondrial respiration (Figure S4G).

Genetic Variation at rs4743771 Controls the Effects of Rosi Treatment on Cholesterol Metabolism in Diabetic Patients

In genome-wide association studies, the A allele of rs4743771 was associated with a higher body fat percentage (p = 0.006, effect = 0.017 SD/allele), as previously observed in a large-scale meta-analysis on body fat percentage (N = 74,388) (Lu et al., 2016). While no association was observed with BMI in the overall population (p = 0.18) (Locke et al., 2015), we found that the rs4743771 A allele was associated with a higher BMI in

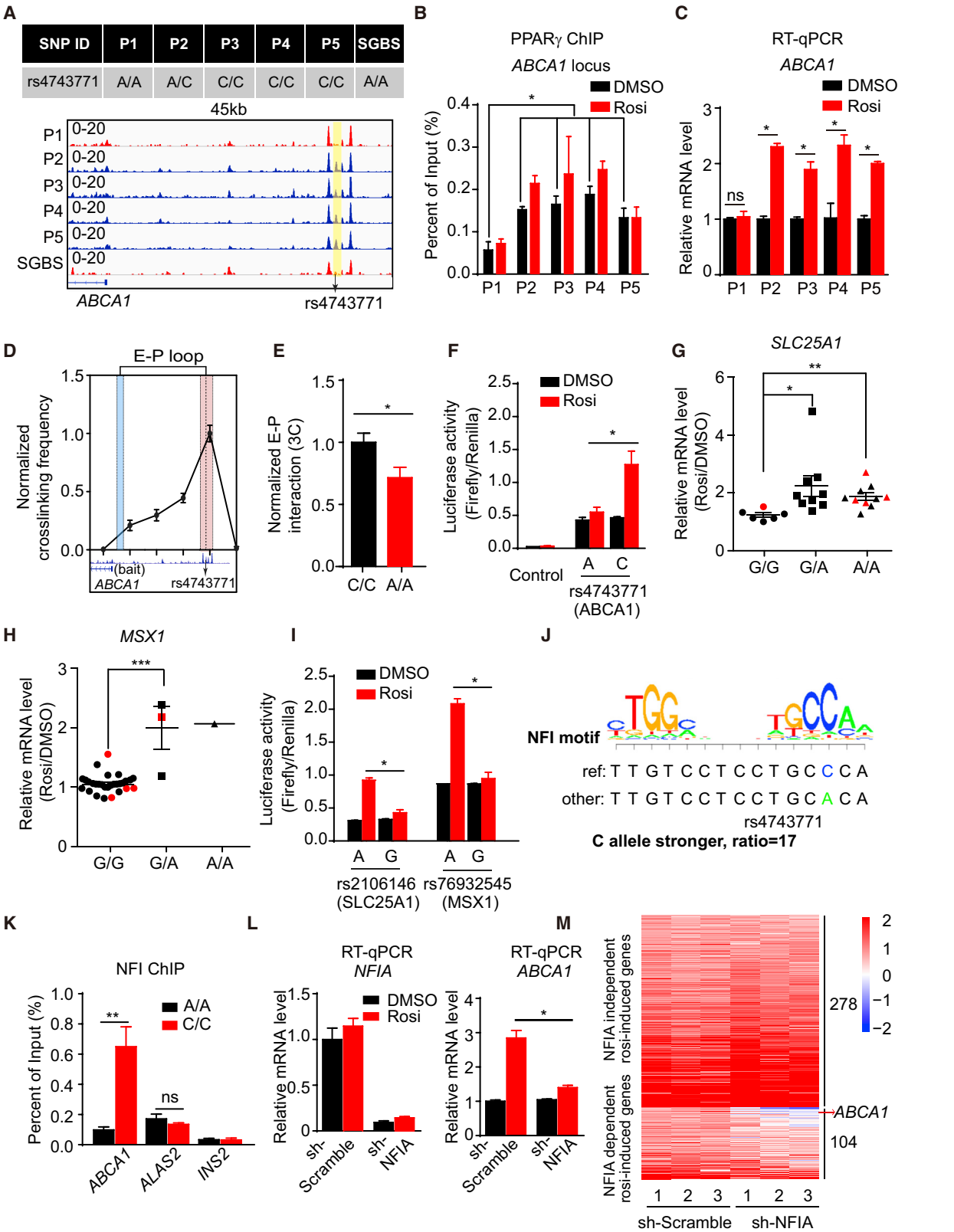

Figure 3. Genetic Variants Determine Differential PPARγ Occupancy by Modulating Binding of NFIA

(A) The genotype of rs4743771 in all five patients and the SGBS cell line (top). Visualization of a P1-specific absent peak region (yellow box) at *ABCA1* loci across patients and the SGBS cell line (bottom panel). Black arrow indicates the position of rs4743771.

(legend continued on next page)

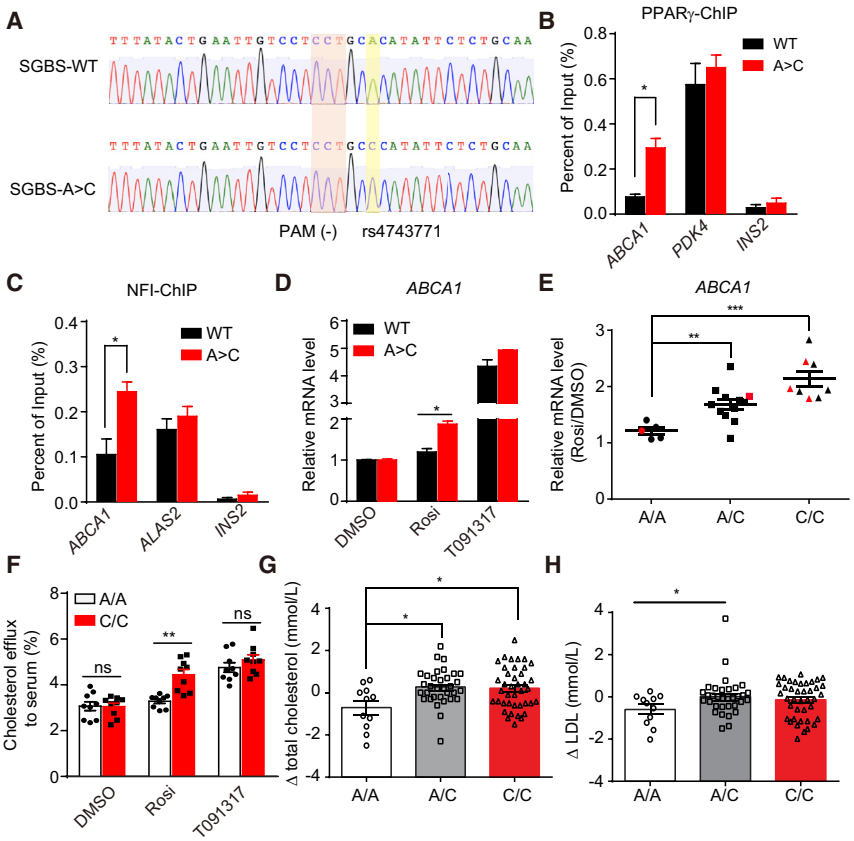

Figure 4. Genetic Variants Determine and Predict Individual Differences in Rosi Responsiveness

(A) Sanger sequencing validation of the A/A allele to C/C allele correction.

(B and C) PPARγ (B) and NFI (C) ChIP-qPCR for *ABCA1*, *PDK4*, *ALAS2*, and *INS2* in SGBS wild-type (WT) and SGBS A > C adipocytes.

(D) mRNA expression of *ABCA1* in SGBS WT and SGBS A > C adipocytes treated with DMSO, 1 μM rosi, or 10 μM T091317 (n = 3).

(E) mRNA expression of *ABCA1* in hASC-derived adipocytes from 25 patients. Red dots represent patients P1-P5. Data are expressed as mean ± SEM fold change due to rosi.

(F) Cholesterol efflux to serum in 3 patient adipocytes carrying A/A and 3 patient adipocytes carrying C/C treated with DMSO, 1 μM rosi, or 10 μM T091317 (n = 3).

(G and H) The change of total cholesterol (G) and LDL (H) levels after rosi treatment in patients carrying different rs4743771 genotypes.

qRT-PCR, ChIP-qPCR data are expressed as mean ± SEM. *p < 0.05; **p < 0.01; ***p < 0.001; ns, p > 0.05 (Student's t test).

See also Figure S4.

physically inactive individuals (p = 0.003, effect = 0.030 SD/allele, N = 42,066), and this association was even more pronounced among women (p = 0.0002, effect = 0.048 SD/allele, N = 26,836) (Graff et al., 2017).

These findings are intriguing and suggest a role for rs4743771 in regulating fat cell mass, but they do not address the more specific question of whether genetic variation in rs4743771 has relevance to the effects of rosi on serum cholesterol levels. It is well established that rosi treatment leads to increases in total as well as low-density lipoprotein (LDL) cholesterol (Rosenblit, 2016). The mechanism is not well understood, but this hypercholesterolemic response is thought to be an adverse effect of rosi that may contribute to myocardial infarctions and strokes among patients taking the drug (Graham et al., 2010).

We interrogated the clinical relevance of SNP rs4743771 in a cohort of 84 diabetic patients whose serum chemistries were studied before and after treatment with rosi for 48 weeks (Wang et al., 2008). The patients were blindly genotyped, and then genotype-phenotype analysis was performed. Remarkably, the increase in levels of total cholesterol (Figure 4G) and LDL cholesterol (Figure 4H) in response to rosi was higher in diabetic patients whose genomes contained one or two copies of the rs4743771 C allele than in patients with the A allele. Increased cholesterol levels are a well-described adverse effect of rosi, which has been mechanistically linked to increased *ABCA1* gene expression in preclinical studies (Vaisman et al., 2001). No rs4743771 genotype altered the beneficial effects of rosi on hemoglobin A1c (Figure S4H) and fasting glucose levels (Figure S4I). Thus, patients with the rs4743771 A/A genotype get the glycemic benefits of rosi with a lower likelihood of experiencing the adverse consequence of elevated cholesterol, suggesting a way forward in identifying

(B) PPARγ ChIP-qPCR for *ABCA1* in all five patient adipocytes treated with DMSO or rosi (n = 3).

(C) mRNA expression of *ABCA1* in five patient adipocytes treated with DMSO and rosi (n = 3), normalized to *HPRT*; DMSO was set to 1, as measured by qRT-PCR.

(D) Enhancer-promoter (E-P) loop identified between the region near rs4743771(red) and the *ABCA1* gene promoter (blue) by 3C in C/C patient adipocytes (n = 4).

(E) E-P loop in A/A and C/C patient adipocytes (n = 5). E-P interactions were normalized to the intragenic interaction at the TBP locus.

(F) The activities of luciferase reporters with the different alleles for rs4743771 and control reporter PGL4.24 in 3T3-L1 adipocytes treated with DMSO or 1 μM rosi.

(G and H) mRNA expression of SLC25A1 (G) and MSX1 (H) in hASC-derived adipocytes from 25 patients. Red dots represent patients P1–P5. Data are expressed as mean ± SEM fold change due to rosi.

(I) The activities of luciferase reporters with the different alleles for rs2106146 and rs76932545 in 3T3-L1 adipocytes treated with DMSO or 1 μM rosi.

(J) The putative effect of rs4743771 on NFI binding.

(K) NFI ChIP-qPCR for *ABCA1*, *ALAS2*, and *INS2* in 3 patient adipocytes carrying A/A and 3 patient adipocytes carrying C/C.

(L) mRNA expression of *NFIA* and *ABCA1* in NFIA knocked-down adipocytes treated with rosi (n = 3), normalized to *HPRT*, as measured by qRT-PCR.

(M) Heatmap of rosi-induced genes in control adipocytes and NFIA-depleted adipocytes treated with either DMSO or 1 μM rosi.

qRT-PCR, ChIP-qPCR, luciferase reporter, and 3C data are expressed as mean ± SEM. *p < 0.05; **p < 0.01; ***p < 0.001; ns, p > 0.05 (Student's t test).

See also Figure S4.

individuals with lower risks associated with rosi treatment, which is a cornerstone of personalized pharmacotherapy.

DISCUSSION

By applying unbiased "omics" approaches to patient-specific ASC models, we have determined that genetic variation is enriched at PPARγ sites whose absence or presence is specific to individuals. Importantly, a single SNP that affected rosi regulation of cholesterol metabolism identified patients at risk for adverse effects of rosi in a clinical study. Thus, our data and methodology provide a proof of principle for a mechanistic understanding of how natural genetic variants control individual responses to antidiabetic drugs. These principles could be extended to different cell types, such as macrophages, where PPARγ is relatively abundant and TZDs generally favor an anti-inflammatory alternative activation phenotype (Nelson et al., 2018).

Genetic variants modulate the response to environmental stimuli and drugs in the context of complex diseases (Lee et al., 2014; Soccio et al., 2015). Indeed, several variant annotations in the Pharmacogenomics Knowledgebase have been identified as modulating rosi responsiveness (e.g., *CYP2C8*, *LPIN1*, *PAX4*, and *SLCO1B1*). Mechanistically, genetic variants in *SLO1B1* and *CYP2C8* affect patient plasma rosi concentration (Dawed et al., 2016), as rosi is thought to be transported into the liver by OATP1B1 (encoded by *SLCO1B1*) and metabolized by CYP450 2C8 enzyme (encoded by *CYP2C8*). However, the precise biological mechanisms for other genetic variants are not known. Non-coding SNPs in regulatory regions may affect transcription factor binding and gene expression, thus contributing to the response to drugs. Here, we employed a genome-wide experimental pipeline with integrative analysis of patient hASC-derived adipocytes, which revealed noncoding SNPs that affect PPARγ genomic binding and the response to TZDs.

Our detailed analysis of one PPARγ-binding-disrupting SNP, rs4743771, revealed its association with rosi induction of the *ABCA1* gene. ABCA1 is responsible for the efflux of cholesterol to APOA1 and small high-density lipoprotein (HDL) particles (McNeish et al., 2000), and deletion of *ABCA1* in mouse adipose tissue alters systemic lipid and glucose metabolism (Cuffe et al., 2018). Interestingly, a previous report has also described a coding variant at the *ABCA1* locus that affects the efficacy of rosi monotherapy in type 2 diabetes patients (Wang et al., 2008). This highlights the power of our approach to identify new non-coding genetic variants controlling drug responses. Rosi has been associated with increased LDL and total cholesterol in diabetic patients (Rosenblit, 2016), and these adverse lipid changes have been suggested to promote myocardial infarction and stroke in patients treated with rosi. We find that rosi did not increase LDL and total cholesterol in A/A patients while maintaining its beneficial effects on glucose metabolism.

With a minor allele frequency of 0.4, the A/A genotype of rs4743771 represents ~16% of patients. Considering the millions of patients with diabetes in the United States (US) alone, this represents a large number of patients for whom rosi therapy might be considered because of the predicted lack of adverse effects on cholesterol with the retention of amelioration of insulin resistance. We have also tested the association between the identified genetic variants (rs2106146 and rs76932545) and individual responsiveness to rosi treatment. However, there are only four G/G patients for rs2106146 and no A/A patients for rs76932545 in the cohort of 84 patients that we examined, so there is insufficient power to examine whether these two SNPs are associated to responsiveness to rosi and the synergic effect of these three SNPs on rosi response.

In summary, our study presents an advanced strategy using stem cell-derived adipocytes to identify human genetic variation that determines patient response to antidiabetic drugs. While the overall effects of drugs are clearly polygenic, the present work demonstrates that individual SNPs can have predictable effects on gene expression and metabolic phenotype.

STAR★METHODS

Detailed methods are provided in the online version of this paper and include the following:

- KEY RESOURCES TABLE
- CONTACT FOR REAGENT AND RESOURCE SHARING
- EXPERIMENTAL MODEL AND SUBJECT DETAILS
  - Primary hASCs
  - SGBS cell line
  - Patients and study design
- METHOD DETAILS
  - Adipogenic differentiation of hASCs and SGBS
  - Oil Red O staining and Immunostaining
  - Western blot and gene expression analysis
  - RNA-seq and data processing
  - Chromatin Immunoprecipitation (ChIP)
  - ChIP-seq and data processing
  - Motif analysis
  - SNaPshot genotyping assay
  - CRISPR/Cas9 editing of SGBS
  - Chromatin conformation capture (3C)
  - Luciferase reporter assay
  - Seahorse assay
  - Cholesterol efflux assay
  - Clinical laboratory tests
  - Genome-wide association studies (GWAS) analysis
  - Genotyping
- QUANTIFICATION AND STATISTICAL ANALYSIS
- DATA AND SOFTWARE AVAILABILITY

SUPPLEMENTAL INFORMATION

Supplemental Information includes four figures and one table and can be found with this article online at https://doi.org/10.1016/j.stem.2018.11.018.

ACKNOWLEDGMENTS

We thank Daniel Cohen, Victoria Nelson, Yong Hoon Kim, and members of the Lazar lab for technical support and valuable discussions. We thank Amrith Rodrigues and Daniel Rader for technical help with the cholesterol efflux assay. We thank Benjamin Voight for early help with genome-wide association studies (GWAS) analysis. We thank the Functional Genomics Core of the Penn Diabetes Research Center (NIH grant P30 DK19525) for next-generation sequencing. For access to adipose tissue from de-identified, clinically phenotyped subjects, we thank Dr. Gary B. Korus of the Penn Metabolic and Bariatric Surgery Program and William Patterson and Julian Hernandez of the Human

Metabolic Tissue Resource of the Penn Institute for Diabetes, Obesity, and Metabolism. This work was supported by the Cox Medical Institute, the JPB Foundation (M.A.L.), and the NIH (grant R01-DK049780 to M.A.L., grant R01-DK098542 to D.J.S., grant K08-DK094968 to R.E.S., and grant F32-DK116519 to D.G.). W.H. was supported by the American Diabetes Association (training grant 1-18-PDF-132).

AUTHOR CONTRIBUTIONS

W.H. and M.A.L. conceptualized the study, interpreted data, and wrote the manuscript, which was revised and approved by all authors. W.H. performed most experiments. C.J. and D.G. performed bioinformatics analysis. A.M., G.N.N., and R.J.F.L. performed the GWAS analysis. P.D. performed Seahorse assays. R.Z., C.H., and W.J. recruited the patients and collected the clinical data. D.J.S. and R.E.S. assisted with data analysis.

DECLARATION OF INTERESTS

M.A.L. is an advisory board member at Eli Lilly and Pfizer and a consultant to Madrigal Pharmaceuticals and Novartis. G.N.N. is a cofounder and board member of Renalytix AI and consultant to Renalytix AI, PulseData, and BioVie. The remaining authors declare no competing interests.

Received: June 8, 2018
Revised: October 4, 2018
Accepted: November 14, 2018
Published: January 10, 2019

REFERENCES

Caballero, B. (2007). The global epidemic of obesity: an overview. Epidemiol. Rev. *29*, 1–5.

Chawla, A., and Lazar, M.A. (1994). Peroxisome proliferator and retinoid signaling pathways co-regulate preadipocyte phenotype and survival. Proc. Natl. Acad. Sci. USA *91*, 1786–1790.

Chawla, A., Boisvert, W.A., Lee, C.H., Laffitte, B.A., Barak, Y., Joseph, S.B., Liao, D., Nagy, L., Edwards, P.A., Curtiss, L.K., et al. (2001). A PPAR gamma-LXR-ABCA1 pathway in macrophages is involved in cholesterol efflux and atherogenesis. Mol. Cell *7*, 161–171.

Cuffe, H., Liu, M., Key, C.C., Boudyguina, E., Sawyer, J.K., Weckerle, A., Bashore, A., Fried, S.K., Chung, S., and Parks, J.S. (2018). Targeted deletion of adipocyte Abca1 (ATP-binding cassette transporter A1) impairs diet-induced obesity. Arterioscler. Thromb. Vasc. Biol. *38*, 733–743.

Dawed, A.Y., Donnelly, L., Tavendale, R., Carr, F., Leese, G., Palmer, C.N., Pearson, E.R., and Zhou, K. (2016). CYP2C8 and SLCO1B1 variants and therapeutic response to thiazolidinediones in patients with type 2 diabetes. Diabetes Care *39*, 1902–1908.

Dispirito, J.R., Fang, B., Wang, F., and Lazar, M.A. (2013). Pruning of the adipocyte peroxisome proliferator-activated receptor γ cistrome by hematopoietic master regulator PU.1. Mol. Cell. Biol. *33*, 3354–3364.

Fischer-Posovszky, P., Newell, F.S., Wabitsch, M., and Tornqvist, H.E. (2008). Human SGBS cells - a unique tool for studies of human fat cell biology. Obes. Facts *1*, 184–189.

Graff, M., Scott, R.A., Justice, A.E., Young, K.L., Feitosa, M.F., Barata, L., Winkler, T.W., Chu, A.Y., Mahajan, A., Hadley, D., et al.; CHARGE Consortium; EPIC-InterAct Consortium; PAGE Consortium (2017). Genome-wide physical activity interactions in adiposity: a meta-analysis of 200,452 adults. PLoS Genet. *13*, e1006528.

Graham, D.J., Ouellet-Hellstrom, R., MaCurdy, T.E., Ali, F., Sholley, C., Worrall, C., and Kelman, J.A. (2010). Risk of acute myocardial infarction, stroke, heart failure, and death in elderly Medicare patients treated with rosiglitazone or pioglitazone. JAMA *304*, 411–418.

Grant, C.E., Bailey, T.L., and Noble, W.S. (2011). FIMO: scanning for occurrences of a given motif. Bioinformatics *27*, 1017–1018.

Heinz, S., Benner, C., Spann, N., Bertolino, E., Lin, Y.C., Laslo, P., Cheng, J.X., Murre, C., Singh, H., and Glass, C.K. (2010). Simple combinations of lineage-determining transcription factors prime cis-regulatory elements required for macrophage and B cell identities. Mol. Cell *38*, 576–589.

Hiraike, Y., Waki, H., Yu, J., Nakamura, M., Miyake, K., Nagano, G., Nakaki, R., Suzuki, K., Kobayashi, H., Yamamoto, S., et al. (2017). NFIA co-localizes with PPARγ and transcriptionally controls the brown fat gene program. Nat. Cell Biol. *19*, 1081–1092.

Hlouschek, J., Hansel, C., Jendrossek, V., and Matschke, J. (2018). The mitochondrial citrate carrier (SLC25A1) sustains redox homeostasis and mitochondrial metabolism supporting radioresistance of cancer cells with tolerance to cycling severe hypoxia. Front. Oncol. *8*, 170.

Huang da, W., Sherman, B.T., and Lempicki, R.A. (2009). Systematic and integrative analysis of large gene lists using DAVID bioinformatics resources. Nat. Protoc. *4*, 44–57.

Kim, D., Langmead, B., and Salzberg, S.L. (2015). HISAT: a fast spliced aligner with low memory requirements. Nat. Methods *12*, 357–360.

Langmead, B., and Salzberg, S.L. (2012). Fast gapped-read alignment with Bowtie 2. Nat. Methods *9*, 357–359.

Lee, M.N., Ye, C., Villani, A.C., Raj, T., Li, W., Eisenhaure, T.M., Imboywa, S.H., Chipendo, P.I., Ran, F.A., Slowikowski, K., et al. (2014). Common genetic variants modulate pathogen-sensing responses in human dendritic cells. Science *343*, 1246980.

Li, H., Handsaker, B., Wysoker, A., Fennell, T., Ruan, J., Homer, N., Marth, G., Abecasis, G., and Durbin, R.; 1000 Genome Project Data Processing Subgroup (2009). The Sequence Alignment/Map format and SAMtools. Bioinformatics *25*, 2078–2079.

Liao, Y., Smyth, G.K., and Shi, W. (2014). featureCounts: an efficient general purpose program for assigning sequence reads to genomic features. Bioinformatics *30*, 923–930.

Locke, A.E., Kahali, B., Berndt, S.I., Justice, A.E., Pers, T.H., Day, F.R., Powell, C., Vedantam, S., Buchkovich, M.L., Yang, J., et al.; LifeLines Cohort Study; ADIPOGen Consortium; AGEN-BMI Working Group; CARDIOGRAMplusC4D Consortium; CKDGen Consortium; GLGC; ICBP; MAGIC Investigators; MuTHER Consortium; MIGen Consortium; PAGE Consortium; ReproGen Consortium; GENIE Consortium; International Endogene Consortium (2015). Genetic studies of body mass index yield new insights for obesity biology. Nature *518*, 197–206.

Lu, Y., Day, F.R., Gustafsson, S., Buchkovich, M.L., Na, J., Bataille, V., Cousminer, D.L., Dastani, Z., Drong, A.W., Esko, T., et al. (2016). New loci for body fat percentage reveal link between adiposity and cardiometabolic disease risk. Nat. Commun. *7*, 10495.

McNeish, J., Aiello, R.J., Guyot, D., Turi, T., Gabel, C., Aldinger, C., Hoppe, K.L., Roach, M.L., Royer, L.J., de Wet, J., et al. (2000). High density lipoprotein deficiency and foam cell accumulation in mice with targeted disruption of ATP-binding cassette transporter-1. Proc. Natl. Acad. Sci. USA *97*, 4245–4250.

Nelson, V.L., Nguyen, H.C.B., Garcìa-Cañaveras, J.C., Briggs, E.R., Ho, W.Y., DiSpirito, J.R., Marinis, J.M., Hill, D.A., and Lazar, M.A. (2018). PPARγ is a nexus controlling alternative activation of macrophages via glutamine metabolism. Genes Dev. *32*, 1035–1044.

Oram, J.F., and Lawn, R.M. (2001). ABCA1. The gatekeeper for eliminating excess tissue cholesterol. J. Lipid Res. *42*, 1173–1179.

Pertea, M., Pertea, G.M., Antonescu, C.M., Chang, T.C., Mendell, J.T., and Salzberg, S.L. (2015). StringTie enables improved reconstruction of a transcriptome from RNA-seq reads. Nat. Biotechnol. *33*, 290–295.

Pospisilik, J.A., Schramek, D., Schnidar, H., Cronin, S.J., Nehme, N.T., Zhang, X., Knauf, C., Cani, P.D., Aumayr, K., Todoric, J., et al. (2010). Drosophila genome-wide obesity screen reveals hedgehog as a determinant of brown versus white adipose cell fate. Cell *140*, 148–160.

Quinlan, A.R., and Hall, I.M. (2010). BEDTools: a flexible suite of utilities for comparing genomic features. Bioinformatics *26*, 841–842.

Rao, S.S., Huntley, M.H., Durand, N.C., Stamenova, E.K., Bochkov, I.D., Robinson, J.T., Sanborn, A.L., Machol, I., Omer, A.D., Lander, E.S., and Aiden, E.L. (2014). A 3D map of the human genome at kilobase resolution reveals principles of chromatin looping. Cell *159*, 1665–1680.

Robinson, J.T., Thorvaldsdóttir, H., Winckler, W., Guttman, M., Lander, E.S., Getz, G., and Mesirov, J.P. (2011). Integrative genomics viewer. Nat. Biotechnol. *29*, 24–26.

Rosenblit, P.D. (2016). Common medications used by patients with type 2 diabetes mellitus: what are their effects on the lipid profile? Cardiovasc. Diabetol. *15*, 95.

Sears, D.D., Hsiao, G., Hsiao, A., Yu, J.G., Courtney, C.H., Ofrecio, J.M., Chapman, J., and Subramaniam, S. (2009). Mechanisms of human insulin resistance and thiazolidinedione-mediated insulin sensitization. Proc. Natl. Acad. Sci. USA *106*, 18745–18750.

Soccio, R.E., Tuteja, G., Everett, L.J., Li, Z., Lazar, M.A., and Kaestner, K.H. (2011). Species-specific strategies underlying conserved functions of metabolic transcription factors. Mol. Endocrinol. *25*, 694–706.

Soccio, R.E., Chen, E.R., and Lazar, M.A. (2014). Thiazolidinediones and the promise of insulin sensitization in type 2 diabetes. Cell Metab. *20*, 573–591.

Soccio, R.E., Chen, E.R., Rajapurkar, S.R., Safabakhsh, P., Marinis, J.M., Dispirito, J.R., Emmett, M.J., Briggs, E.R., Fang, B., Everett, L.J., et al. (2015). Genetic variation determines PPARγ function and anti-diabetic drug response in vivo. Cell *162*, 33–44.

Step, S.E., Lim, H.W., Marinis, J.M., Prokesch, A., Steger, D.J., You, S.H., Won, K.J., and Lazar, M.A. (2014). Anti-diabetic rosiglitazone remodels the adipocyte transcriptome by redistributing transcription to PPARγ-driven enhancers. Genes Dev. *28*, 1018–1028.

Ussar, S., Lee, K.Y., Dankel, S.N., Boucher, J., Haering, M.F., Kleinridders, A., Thomou, T., Xue, R., Macotela, Y., Cypess, A.M., et al. (2014). ASC-1, PAT2, and P2RX5 are cell surface markers for white, beige, and brown adipocytes. Sci. Transl. Med. *6*, 247ra103.

Vaisman, B.L., Lambert, G., Amar, M., Joyce, C., Ito, T., Shamburek, R.D., Cain, W.J., Fruchart-Najib, J., Neufeld, E.D., Remaley, A.T., et al. (2001). ABCA1 overexpression leads to hyperalphalipoproteinemia and increased biliary cholesterol excretion in transgenic mice. J. Clin. Invest. *108*, 303–309.

Wang, J., Bao, Y.Q., Hu, C., Zhang, R., Wang, C.R., Lu, J.X., Jia, W.P., and Xiang, K.S. (2008). Effects of ABCA1 variants on rosiglitazone monotherapy in newly diagnosed type 2 diabetes patients. Acta Pharmacol. Sin. *29*, 252–258.

STAR★METHODS

KEY RESOURCES TABLE

REAGENT or RESOURCE	SOURCE	IDENTIFIER
Antibodies		
PPARγ	Santa Cruz Biotechnology	Cat# sc-7196, RRID: AB_654710
FABP4	R & D Systems	Cat# AF3150, RRID: AB_2278261
NFI	Santa Cruz Biotechnology	Cat# sc-74445X, RRID: AB_2153046
Tubulin-HRP	Abcam	Cat# ab21058, RRID: AB_ 727045
Chemicals and Reagents		
DMEM	Thermo Fisher Scientific	Cat# 11995065
DMEM/F12	Thermo Fisher Scientific	Cat# 11330032
Fetal bovine serum	Atlanta Biologicals	Cat# S11150
Insulin solution human	Sigma	Cat# I9278
3-Isobutyl-1-methylxanthine	Sigma	Cat# I5879
Dexamethasone	Sigma	Cat# D4902
Indomethacin	Sigma	Cat# I7378
Rosiglitazone	Sigma	Cat# R2408
Biotin	Sigma	Cat# B4639
Pantothenate	Sigma	Cat# P5155
Insulin-Transferrin-Selenium	Thermo Fisher Scientific	Cat# 41400045
Hydrocortisone	Sigma	Cat# H0888
Triiodothyronine	Sigma	Cat# T6397
T091317	Sigma	Cat# T2320
Paraformaldehyde Solution, 4%	Affymetrix	Cat# 19943 1 LT
SuperScript II Reverse Transcriptase	Thermo Fisher Scientific	Cat# 18064014
cOmplete, EDT-free Protease Inhibitor Cocktail	Roche	Cat# 11873580001
Chloroform	Sigma	Cat# C2432-500ML
RNase A (DNase and Protease Free)	Fermentas Life Sciences	Cat# EN0531
Phenol/Chloroform/ Isoamyl Alcohol	Fisher Scientific	Cat# BP1753I-400
ChIP DNA Clean & Concentrator- Capped column	Zymo Research	Cat# D5205
DNA LoBind Microcentrifuge Tube	Eppendorf	Cat# 30108.051
Deoxynucleotide (dNTP) Solution Mix	New England Biolabs	Cat# N0447S
Phusion Hot Start II DNA Polymerase	Thermo Fisher Scientific	Cat# F-549L
UltraPure Glycogen	Thermo Fisher Scientific	Cat# 10814010
T4 DNA Polymerase	New England Biolabs	Cat# M0203S
Klenow Fragment	New England Biolabs	Cat# M0212S
Klenow DNA Polymerase	New England Biolabs	Cat# M0210S
T4 Polynucleotide Kinase	New England Biolabs	Cat# M0201S
ExoSAP-IT	Affymetrix	Cat# 78201.1.ML
Calf Intestinal Phosphatase	New England Biolabs	Cat# M0290S
Human serum	Millipore Sigma	Cat# S1-100ML
[1,2-3H(N)]-Cholesterol	Perkin Elmer	Cat# NET139250UC
Lipofectamine 3000	Thermo Fisher Scientific	Cat# L3000008
EcoRI-HF	New England Biolabs	Cat# R3101L
T4 DNA Ligase	New England Biolabs	Cat# M0202
Sodium Pyruvate	Thermo Fisher Scientific	Cat# 11360070
D-(+)-Glucose solution	Sigma	Cat# G8769
L-Glutamine	Thermo Fisher Scientific	Cat# 25030081

(*Continued on next page*)

Continued

REAGENT or RESOURCE	SOURCE	IDENTIFIER
Critical Commercial Assays		
RNeasy Mini Kit	QIAGEN	Cat# 74106
High-Capacity cDNA Reverse Transcription Kit	Applied Biosystems	Cat# 4368813
Power SYBR Green PCR Master Mix	Applied Biosystems	Cat# 4367659
Agilent high sensitivity DNA assay	Agilent	Cat# 5067-4626
Agencourt AMPure XP beads	Beckman Coulter	Cat# A63881
Illumina TruSeq stranded Total RNA Library Prep Kit	Illumina	Cat# RS-122-2303
SNaPshot Multiplex Kit	Thermo Fisher Scientific	Cat# 4323159
Seahorse XF cell mito stress test kit	Agilent Technologies	Cat# 103015-100
TaqMan Gene Expression Master Mix	Thermo Fisher Scientific	Cat# 4369016
Dual-Luciferase® Reporter Assay System	Promega	Cat# E1910
Pierce BCA Protein Assay Kit	Thermo Fisher Scientific	Cat# 23225
Deposited Data		
RNA-seq	This study	GEO: GSE 115421
PPARγ ChIP-seq	This study	GEO: GSE 115421
PPARγ ChIP-seq in SGBS	(Soccio et al., 2011)	GEO: GSE25836
Recombinant DNA		
pGuide	Addgene	Cat# 44719
pCas9_GFP	Addgene	Cat# 64711
pGL4.24 Vector	Promega	Cat# E842A
TRC Lentiviral Non-targeting shRNA Control	Dharmacon	Cat# RHS6848
TRC Lentiviral Human NFIA shRNA	Dharmacon	Cat# RHS4533-EG4774
psPAX2	Addgene	Cat# 12260
pCMV-VSV-G	Addgene	Cat# 8454
BAC ABCA1	CHORI	Cat# RP11-1N10
BAC TBP	CHORI	Cat# RP11-794H3
Oligonucleotides		
See Table S1	N/A	N/A
Software and Algorithms		
Bowtie 2.3.0	(Langmead and Salzberg, 2012)	http://bowtie-bio.sourceforge.net/bowtie2/manual.shtml
SAMtools 1.8	(Li et al., 2009)	http://samtools.sourceforge.net/
Bedtools 2.26.0	(Quinlan and Hall, 2010)	http://bedtools.readthedocs.io/en/latest/
Homer v4.9	(Heinz et al., 2010)	http://homer.ucsd.edu/homer/
R 3.3.2		www.r-project.org/
StringTie 1.3.3b	(Pertea et al., 2015)	https://ccb.jhu.edu/software/stringtie/
Hisat2 2.0.5	(Kim et al., 2015)	https://ccb.jhu.edu/software/hisat2/index.shtml
IGV 2.4	(Robinson et al., 2011)	http://software.broadinstitute.org/software/igv
MEME SUITE 4.12.0	(Grant et al., 2011)	http://meme-suite.org/
FeatureCounts 1.5.1	(Liao et al., 2014)	http://bioinf.wehi.edu.au/featureCounts/
DAVID Bioinformatics Resources 6.8	(Huang da et al., 2009)	https://david.ncifcrf.gov/

CONTACT FOR REAGENT AND RESOURCE SHARING

Further information and request for resources and reagents should be directed to and will be fulfilled by the Lead Contact, Mitchell A. Lazar, M.D., Ph.D. (lazar@pennmedicine.upenn.edu)

EXPERIMENTAL MODEL AND SUBJECT DETAILS

Primary hASCs

For hASCs isolation, abdominal subcutaneous adipose tissues around the umbilical area were obtained from obese individuals with participant informed consent obtained after the nature and possible consequences of the studies were explained under protocols approved by the Institutional Review Boards of the Perelman School of Medicine at the University of Pennsylvania. The fat biopsies were digested using 0.1% collagenase type IA at 37°C for 30-60 min. Afterward, the aliquots of the infranatant containing the stromal vascular fraction (SVF) were pelleted at 1,200 × g for 10 min. The pellet was resuspended in DMEM (ThermoFisher, 11995-065) supplemented with 10% fetal bovine serum (Atlanta Biologicals, S11150) and penicillin/streptomycin, and flited through a 100-μm filter (Falcon). The cells were maintained in DMEM medium at 37°C with 5% CO2 and passaged 3-4 times before adipogenic differentiation.

SGBS cell line

SGBS preadipocytes were cultured in DMEM/F12 (ThermoFisher, 11330-032) supplemented with 10% fetal bovine serum (Atlanta Biologicals, S11150), 1% penicillin/streptomycin, 33 μM biotin and 17 μM pantothenate.

Patients and study design

Patients and study design was as previously described (Wang et al., 2008). The study was approved by the institutional review board of Shanghai Jiao Tong University Affiliated Sixth People's Hospital (Shanghai, China). Each patient provided written informed consent before participating in the study.

A total of 105 newly diagnosed patients with type 2 diabetes, defined according to the World Health Organization criteria, were derived from the outpatient clinics at 10 hospitals in Shanghai. All patients were naive to prior antidiabetic therapy and treated with rosiglitazone for 48 weeks. Enrolled patients were 30–70 years of age, glycated hemoglobin $\geq$ 6.5%, and a body mass index (BMI) $\geq$ 18.5 kg/m2. For the female patients, postmenopause, surgical sterilization, or effective contraception was required. Exclusion criteria were: (i) type 1 diabetes, gestational diabetes, or other specific types; (ii) acute or chronic complications in need of insulin therapy; (iii) significant cardiocerebral, hepatic or nephric disease; (iv) malignant tumor, hematological disease, autoimmune disease, psychiatric disease, or significant digestion and absorption disturbances; (v) current exposure to medication affecting glucose metabolism, such as glucocorticoid; (vi) long-term alcohol or drug abuse; (vii) fasting plasma glucose > 13 mmol/L (234 mg/dL) and/or 2 h post-load plasma glucose > 18 mmol/L (364 mg/dL); and (viii) blood pressure > 180/110 mmHg.

The initial dose was 4 mg/d and escalated to 8 mg/d in patients who failed to attain glycemic targets of fasting plasma glucose > 7 mmol/L (126 mg/dL) and/or 2 h plasma glucose > 11 mmol/L (200 mg/dL). Patients with glycated hemoglobin was $\geq$ 8% or fasting plasma glucose > 13 mmol/L (234 mg/dL) or 2 h plasma glucose > 18 mmol/L (364 mg/dL) twice (a maximal interval of 6 d) were withdrawn from the study, so the results of 93 patients were included in the original study (Wang et al., 2008). The present study analyzed 84 patients, because two patients' genomic DNA was not available after 10 years' use and seven patients did not have lipids profile data.

METHOD DETAILS

Adipogenic differentiation of hASCs and SGBS

hASCs at passage P3-P4 were cultured in DMEM medium. Confluent hASCs were then transferred into adipogenic medium for 14 days. Adipogenic medium formulation was as follows: DMEM with 10% FBS, 1% penicillin/streptomycin, dexamethasone (1 μM), IBMX (0.5 mM), indomethacin (0.2mM), Insulin (10 μg/ml) and rosiglitazone (1 μM). Then, cells were further cultured in maintenance medium for another 7 days. Maintenance medium formulation was as follows: DMEM with 10% FBS, 1% penicillin/streptomycin, dexamethasone (1 μM), IBMX (0.5 mM), indomethacin (0.2mM) and Insulin (10 μg/ml).

For adipogenic differentiation of SGBS cells, confluent SGBS cells were cultured in DMEM/F12 (ThermoFisher, 11330-032) supplemented with 1% penicillin/streptomycin, 33 μM biotin, 17 μM pantothenate, 1% Insulin-Transferrin-Selenium (ThermoFisher, 41400-045), 100 nM hydrocortisone, 0.2 nM triiodothyronine, 25 nM dexamethasone, 0.5 mM IBMX and 1 μM rosiglitazone. After 4 days, the medium was changed to differentiation medium without dexamethasone, IBMX and rosiglitazone for 10 days. Medium was changed every 2-3 days.

Oil Red O staining and Immunostaining

For Oil Red O staining, adipocytes were fixed by 4% PFA solution for 60 min at room temperature (RT). Fixed cells were stained with 0.24% Oil Red O in 40% 2-propanol for 15 min.

For Immunostaining, cells plated on glass coverslips were fixed by 4% PFA solution for 10 min at room temperature. Then cells were incubated in blocking buffer (1% bovine serum albumin in PBS) with 0.5% Triton X-100 for 30 min at RT. Afterward, samples were incubated with primary antibodies at 4°C overnight and then with appropriate fluorescent probe-conjugated secondary antibodies for 1 h at RT. Images were captured with fluorescence microscope.

Western blot and gene expression analysis

For western blot, adipocytes were washed with cold PBS and lysed with Laemmli's sample buffer, and then cell lysates were separated on SDS-PAGE, transferred onto nitrocellulose membrane and blotted with indicated primary antibodies. The membrane was detected by secondary antibody conjugated to HRP.

For gene expression analysis, total RNA samples were collected with RNeasy kit (QIAGEN) according to manufacturer's instructions. The RNA for each reaction was reverse-transcribed to cDNA using High-Capacity cDNA Reverse Transcription Kit. Quantitative real-time PCR was subsequently conducted with specific primers and Power SYBR Green PCR Master Mix (Applied Biosystems). The relative expression levels were normalized against the internal control (HPRT). Primers used were listed in Table S1.

RNA-seq and data processing

The RNA samples from independent experiments were processed with the Ribo-Zero rRNA Removal Kit (Epicenter Biotechnologies) to reduce ribosomal RNA abundance, prepared with the TruSeq RNA Sample Prep Kit (Illumina) and sequenced single-end at 100bp read length on Illumina HiSeq2000 by the Functional Genomics Core of the Penn Diabetes Research Center or sequenced paired-end at 150bp read length by Novogene.

RNA-seq reads were aligned to human reference genome (hg19) using Hisat2 with default parameters. Only unique mapped reads were considered for further analysis. Normalized expression value, fragments per kilobase of exon per million reads mapped (FPKM), was calculated for each gene using StringTie. A gene was considered expressed if its expression value is larger than 1 in at least one subject, and there were 16,961 expressed genes (12001 expressed protein-coding genes). For differential expression analysis, raw read counts were measured within Ensembl genes (GRCH37.75) using featureCounts, and then edgeR pipeline was used with adjusted p value (Benjamini Hochberg) $\leq$ 0.01 and fold change > 1.5 from samples treated with rosi against samples treated with DMSO for each patient. Differentially expressed genes with fold change > 1.5 in only one patient were defined as patient-specific responsive genes. In contrast, differentially expressed genes with fold change < 1.5 in only one patient were defined as patient-specific unresponsive genes. Genes with fold change > 1.5 in all five patients were defined as common responsive genes. GO and KEGG enrichment analysis were performed using DAVID Bioinformatics Resources v6.8. The same pipeline was used for RNA-seq data from NFIA-depleted samples. Differentially expressed genes were identified between samples treated with rosi against samples treated with DMSO with adjusted p value $\leq$ 0.01 and fold change > 1.5.

To compare gene expression pattern in adipocytes and adipose tissues, FPKM value of each gene in each sample was transformed by log2 before analysis. Differentially expressed genes between groups were identified by one-way analysis of variance (ANOVA) with p value < 0.02, followed by principal component analysis (PCA) analysis.

Chromatin Immunoprecipitation (ChIP)

ChIP assays were performed as described previously (Dispirito et al., 2013). Briefly, mature adipocytes or human adipose tissues were crosslinked in 1% formaldehyde for 15 min followed by quenching with 1/20 volume of 2.5 M glycine solution for 5 min. Soluble chromatin was prepared following sonication and then was incubated with anti-PPARγ antibody (Santa-Cruz) or anti-NFI antibody (Santa-Cruz). Crosslinking was reversed overnight at 65°C in SDS buffer (50 mM Tris-HCL, 10 mM EDTA, 1% SDS at pH 8), and DNA was purified using phenol/chloroform/isoamyl alcohol. Precipitated DNA was analyzed by qPCR or next-generation sequencing.

ChIP-seq and data processing

ChIP experiments were performed independently on mature human adipocytes or human adipose tissues. DNA was amplified according to the ChIP-seq sample preparation guide provided by Illumina using adaptor oligo and primers from Illumina, enzymes from New England Biolabs, and PCR purification kit and MinElute kit from QIAGEN. ChIP-seq libraries were sequenced single-end at 50bp read length on Illumina HiSeq2000 by the Functional Genomics Core of the Penn Diabetes Research Center.

ChIP-seq reads were aligned to human reference genome (hg19) using Bowtie2. Only unique mapped reads were considered for further analysis. Aligned reads from biological replicates were pooled together and peak calling was performed by HOMER with normalized tag count $\geq$ 6, p value < 0.00001 and fold change $\geq$ 4. Afterward, peaks from each patient were merged together using BEDTools, and then resized to 200 bp. Normalized read counts was calculated using HOMER for each peak in each patient. Peaks were defined as patient-specific peaks only if the read counts in one patient is at least 2 times stronger than all other four patients. In contrast, peaks were defined as patient-specific absent peaks only if the read counts in one patient is at least 0.5 times weaker than all other four patients. Peaks with normalized reads counts larger than 8 in all five patients were defined as common PPARγ peaks. GO and KEGG enrichment analysis were performed using DAVID Bioinformatics Resources v6.8 based on the nearby genes within 10kb. Browser tracks were processed by Homer v4.9 and visualized on Integrative Genomics Viewer (IGV). Each differential peak was associated with the closest TSS (within 200 kb) of patient-specific genes identified in RNA-seq as described above. A random test was performed by shuffling gene/peak label 3000 times to compare the differential peak-gene association. To assess if SNPs are enriched in patient-specific PPARγ peaks, a random test by shuffling peak label 3000 times was performed. To compare PPARγ binding sites in adipocytes and adipose tissues, normalized tag counts of PPARγ binding site in each sample were transformed by log2 before analysis. Differentially PPARγ binding sties between groups were identified by one-way ANOVA with p value < 0.05, followed by PCA analysis.

Motif analysis

To find SNPs within patient-specific unique/absent PPARγ binding sites affecting PPARγ motif or its cooperating factors NFI, CEBPα and GR motifs, the position weighted matrixes (PWMs) of these motifs coming from Homer and MEME were used. For each SNP in patient-specific unique/absent PPARγ binding sites, the hg19 reference sequence for 20bp on either side was retrieved, and this was modified to generate the new sequences by replacing the base at reference sequence with its counterpart alleles. A FASTA file with these sequences was interrogated for each PWMs using FIMO algorithm in MEME suite with p value < 0.001. FIMO assigns p value to each sequence for PWMs and points out the coordinate of motifs at each sequence. The SNPs with position weight at a PWM larger than 0.3 and with the ratio of the position weights between two genotypes of the SNP larger than 3 were considered.

SNaPshot genotyping assay

Genotyping were carried out with SNaPshot Multiplex Kit (Applied Biosystem) according to manufacturer's instructions. Briefly, each region of interest flanking the SNP was PCR amplified, and 5 μL of PCR product was purified by ExoSAP-IT reagent (Affmetrix). Primer extension was performed by adding 1 μL of purified PCR product to a mix of 2.5 μL SNaPshot reagent, 1 μL water and 0.2pmol extension primer for 25 cycles on Thermocycler. To remove unincorporated fluorescent dNTPs post-extension, each reaction was incubated 1U of Calf Intestinal Phosphatase (New England BioLabs). Samples were sequenced by the Penn DNA Sequencing Facility on an ABI 3730, and genotypes were identified manually using Peak Scanner Software (Life Technologies).

CRISPR/Cas9 editing of SGBS

The CRISPR/Cas9 expression vector pCas9_GFP and the sgRNA-expression vector pGuide were gifts from Dr. Kiran Musunuru (Addgene plasmid #44719 and #64711). Guide RNAs were designed by manual inspection of the genomic sequences flanking rs4743771, and then constructed in the pGuide plasmid. Next, the pGuide-rs4743771 vector, the pCas9_GFP vector, and the ssODN containing C allele (Integrated DNA Technologies) were co-transfected into the SGBS preadipocyte cell line using the Amaxa-Nucleofector device (program U-033) and the basis nucleofector kit for primary mammalian fibroblasts (Lonza). Cells were dissociated with trypsin 48 h post-transfection, and GFP-positive cells were isolated by FACS (FACSAriaII, BD Biosciences) and replated onto 96-well plate. Subsequently, selected clones were genotyped by PCR and Sanger sequencing.

Chromatin conformation capture (3C)

In situ chromosome conformation capture (3C) samples were prepared as described previously with modifications (Rao et al., 2014). Briefly, 5 million cells were crosslinked with 1% formaldehyde and quenched by 2.5 M glycine. Cells were collected and resuspended in Hi-C lysis buffer (10 mM Tris-HCl pH 8.0, 10 mM NaCl, 0.2% NP-40) with proteinase inhibitor (Sigma). Isolated nuclei were digested with EcoR1 and then ligated. After ligation, the supernatant was removed, the pellet containing nuclei resuspended in Hi-C lysis buffer and residual EcoRI enzymes were denatured by incubating at 65°C for 30 min. The nuclei were spun down for 5 min at 600 g, after which the supernatant was discarded, and the pellet containing nuclei was resuspended again in Hi-C lysis buffer. The nuclei were reversed crosslinked and treated with proteinase overnight. DNA was isolated using phenol/chloroform/isoamyl alcohol and second chloroform wash. Precipitated DNA was dissolved in water, and 100ng of DNA was used for each technical replicate for quantitative PCR with specific TaqMan probes. Standards were prepared using EcoRI digested and randomly ligated DNA fragments from BAC (the CHORI BACPAC Resource Center) spanning an entire locus to be probed. All interactions are normalized to the intragenic interaction at the TBP locus to control for DNA amounts and crosslinking efficiency. The BAC, primers and probes used are listed in Table S1.

Luciferase reporter assay

~200bp human DNA fragments encompassing SNP rs4743771 in the ABCA1 locus, rs2106146 in SLC25A1 locus and rs76932545 in MSX1 locus were synthesized from Integrated DNA Technologies with different SNP genotypes. They were cloned into the XhoI and BglII restriction sites of the pGL4 luciferase reporter (Promega) and sequence-verified. Transient transfections of 3T3-L1 cells 2 days post differentiation were performed in 24-well plates, n = 3 wells per condition, using Lipofectamine 3000 (Invitrogen) to add 400ng of pGL4 luciferase reporter and 2ng of renilla luciferase for normalization. One day later, the cells were treated with 1 μM rosi for 48 hours. The Dual-Luciferase Kit (Promega) was used to measure luciferase activities on a Synergy HT plate reader (Biotek).

Seahorse assay

Cells were uniformly plated in XF96 plates and differentiated for 21 days, then treated with DMSO or 1 μM Rosi for 48 hours. OCR was measured with the Seahorse XF96 extracellular flux analyzer (Agilent). Experiments were conducted in XF medium (non-buffered Seahorse XF base medium supplemented with 10 mM glucose (Sigma), 2 mM L-glutamine (Invitrogen), 2 mM sodium pyruvate (Invitrogen), with OCR measured basally and in response to sequential addition of 2 μM oligomycin, 2 μM FCCP, and 0.5 μM rotenone + antimycin A (Agilent). All Seahorse XF data were normalized to total well protein quantified with Pierce BCA protein kit (Thermo Fisher).

Cholesterol efflux assay

Cholesterol efflux assay was performed as described previously (Pospisilik et al., 2010). Briefly, mature adipocytes derived from different patients were labeled with ^{3}H-cholesterol (2 μCi/mL) (Perkin-Elmer Analytical Sciences) overnight. The labeling medium

was removed and human adipocytes were then equilibrated for an additional 24 h period in the presence or in the absence of either 1 μM rosiglitazone or 10 μM T0901317. ^{3}H-cellular cholesterol efflux to 5% human serum was assessed in serum-free medium for a 4-hour in the presence or absence of either 1 μM rosiglitazone or 10 μM T0901317. Cell lipid was extracted with isopropanol and total cellular ^{3}H-cholesterol was measured by liquid scintillation counting. The efficiency of cholesterol efflux was calculated as 100 x (medium cpm) / (medium cpm + cell cpm).

Clinical laboratory tests

Blood samples were collected after an overnight fast and 2 h after a 75 g oral glucose tolerance test (OGTT). Plasma glucose concentrations were measured using the glucose oxidase-peroxidase method with commercial kits (Shanghai Biological Products Institution, Shanghai, China). Glycated hemoglobin values were determined by high-performance liquid chromatography performed on a Bio-Rad Variant II hemoglobin testing system (Bio-Rad Laboratories, Hercules, CA, USA). Serum lipid profiles, including total cholesterol, triglyceride, high-density lipoprotein cholesterol (HDL-C), and low-density lipoprotein cholesterol (LDL-C) were measured with a type 7600-020 Automated analyzer (Hitachi, Tokyo, Japan). The serum levels of insulin and proinsulin were measured in duplicate at 0, 2, 4, and 6 min after an intravenous injection of 50 mL arginine solution at the concentration of 10%, using radioimmunoassay (Linco Research, St Charles, MO, USA).

Genome-wide association studies (GWAS) analysis

To examine whether SNPs are associated with other traits, we searched publicly available data from previously published large-scale genome-wide association studies (GWAS), using PhenoScanner. PhenoScanner is a comprehensive, curated database that catalogs 65 billion genetic associations, for 150 million unique genetic variants.

Genotyping

Genomic DNA was extracted from peripheral blood leucocytes in the whole-blood samples, amplified and genotyped using Sanger sequencing. The genotyping was performed blindly without knowledge of patient phenotypes.

QUANTIFICATION AND STATISTICAL ANALYSIS

Error bars represent the standard error to mean (SEM), and statistical significance was determined by unpaired two tailed Student t test or one-way ANOVA; a p value of ≤ 0.05 was considered significant. Statistical tests were performed using Prism 6.

DATA AND SOFTWARE AVAILABILITY

The accession number for the RNA-seq and ChIP-seq data reported in this paper is GEO: GSE115421.